Journal of Physics D: Applied Physics

PAPER

Inhibit ammonia volatilization from agriculture and livestock by air plasma-activated water

To cite this article: Mengqi Li *et al* 2024 *J. Phys. D: Appl. Phys.* **57** 395205

IOP Publishing Journal of Physics D: Applied Physics
J. Phys. D: Appl. Phys. **57** (2024) 395205 (13pp) https://doi.org/10.1088/1361-6463/ad5d7a

Inhibit ammonia volatilization from agriculture and livestock by air plasma-activated water

Mengqi Li, Zilan Xiong*, Zhuocheng Song, Weiyi Wang, Zhenguo Hou and Yi Dai

State Key Laboratory of Advanced Electromagnetic Technology, Huazhong University of Science and Technology, Wuhan, Hubei 430074, People's Republic of China

E-mail: zilanxiong@hust.edu.cn and xiongzilan@hotmail.com

Received 3 June 2023, revised 25 June 2024
Accepted for publication 1 July 2024
Published 9 July 2024

Abstract

Ammonia volatilization in agriculture and livestock is a considerable cause of air pollution and a significant way of N loss. In this study, we propose a method of using air plasma-activated water (PAW) to inhibit ammonia volatilization from agriculture and livestock and report the inhibitory effect under different discharge times and concentration gradients. PAW was generated through needle–water discharge, while ammonia waters with different concentrations served as simplified models for ammonia release. The compositions of the gas/liquid products of the PAW and those after mixing with ammonia water were detected and analyzed. It was found that the PAW could effectively inhibit the NH_3 volatilization from ammonia water over a large range of conditions, however, NH_3 volatilization promotion could also happen in some cases. The inhibition rate (IR) generally increased with the longer discharge time of the PAW and decreased with the higher ammonia water concentration. As the discharge time increased, the PAW became more acidic and had more active N components, converting more volatile NH_3 to NH_4^+ when mixed with ammonia water. Finally, a relationship model was developed between the IR and pH of the mixture. The IR basically decreased with the increase of the mixture pH, and reached ∼100% when a PAW with a discharge time of 7.5 min or 10 min was mixed with ammonia water with a mass fraction of 0.15%, or PAW of 10 min mixed with 0.25% ammonia water in this study, with the mixture pH lower than 8. The basic chemical process and possible reaction mechanisms were discussed. The proposed method not only effectively reduces ammonia volatilization but also adds more N elements in the form of NO_3^- and NH_4^+, which further improves fertility.

Keywords: atmospheric pressure air plasma, plasma-activated water, ammonia volatilization, inhibition rate

1. Introduction

The Haber–Bosch (H–B) method is a widely used industrial nitrogen fixation method, which consumes a large amount of energy and causes environmental pollution problems [1, 2]. However, the nitrogen use efficiency (NUE) for the whole world was estimated to be only 35% [3, 4] with nitrogen loss rates sometimes reaching as high as 50% of the applied nitrogen fertilizer [5, 6]. This not only wastes resources but also contributes to significant ammonia pollution. Agriculture and livestock activities are responsible for approximately 80% of airborne ammonia emissions [7, 8]. Excessive nitrogen fertilizer use in agriculture and inadequate treatment of animal slurry accumulation in livestock are key factors contributing to high ammonia emissions [7, 9, 10]. Therefore, it is crucial to

* Author to whom any correspondence should be addressed.

develop methods that improve NUE and reduce ammonia loss. The use of an acidifying animal slurry is a feasible method to reduce ammonia volatilization [11–13], which is based on adding acid or other substances to reduce the pH of an animal slurry to reduce the ammonia volatilization. However, this approach has challenges such as complex preparation, safety concerns, and difficulties in transporting the acidifiers.

As one of the important advances in the development of low-temperature plasmas, plasma-activated water (PAW) obtained from an atmospheric air discharge usually is characterized by abundant discharge products, high energy utilization, easy arraying, high activity, absence of pollution, and relatively convenient preparation [14–17]. PAW has been proven to have good application potential in agriculture and biomedical fields [17–21]. Air PAW exhibits high activity due to the presence of reactive oxygen and nitrogen species (RONSs), among which long-lived species usually include NO_3^-, NO_2^-, and H_2O_2 [17, 22, 23]. Additionally, a substantial amount of H^+ is generated during the reaction process, leading to a decrease in pH. Therefore, using air PAW to acidify animal slurry or fertilizers may also lower pH levels and suppress NH_3 volatilization. Moreover, the addition of more N elements in the form of NO_x^- and the conversion from volatile NH_3 or $NH_3{\cdot}H_2O$ to NH_4^+ can increase fertility. In our previous study, we have proposed a new strategy to capture the volatilized NH_3 by air discharge products in the gas phase and successfully produced reusable NH_4NO_3 particles [24, 25]. When these products are reapplied to the farmland as a nitrogen fertilizer, it can achieve the purpose of 'double nitrogen fixation' and improve the NUE.

The majority of volatilized NH_3 from animal slurry comes from urine, accounting for over 80% of the total emissions [26, 27]. Urea in urine is decomposed by urease produced by microorganisms, resulting in the production of CO_2 and NH_3 [28, 29]. Hydrolyzed urine is usually alkaline and highly volatile due to NH_3 [28, 30]. Moreover, anhydrous ammonia is commonly used as liquid nitrogen fertilizer and is another significant source of volatile NH_3 in agricultural fields [31, 32]. To address safety and corrosion concerns associated with pure anhydrous ammonia, ammonia water with lower concentrations is widely used as a practical alternative for soil injection or irrigation [33].

Therefore, this study proposes the use of air PAW to inhibit NH_3 losses in agriculture and evaluate its inhibition effect under different conditions. Ammonia water with varying concentrations is used to simulate NH_3 volatilization from animal urine or liquid fertilizers. The PAW was generated at different discharge time gradients and mixed with ammonia water of different mass fractions. The gas and liquid products of PAW and the mixtures were then detected. Based on an analysis of the NH_3 emission within the fixed time, the inhibition rate (IR) was calculated. The results and reaction mechanism were then analyzed, and a relationship model was developed to describe the IR and mixed solution pH.

2. Experimental setup and methods

2.1. Experimental setup

A schematic of the experimental setup is shown in figure 1. A homemade high-voltage direct-current (DC) power supply is used to drive the needle–water discharge in the air environment to generate PAW. A stainless-steel needle with a diameter of 4 mm is used as a needle electrode for the power electrode, while 10 ml of deionized water (DIW) in a glass dish (inner diameter ∅55 mm × 15 mm) is used as a water electrode as a ground and copper conductive adhesive is employed to establish a reliable ground connection between the water electrode and the solid-state grounded electrode. The distance between the tip of needle electrode and the surface of DIW is 5 mm. The entire setup is enclosed in a transparent acrylic-sealed container with inner dimensions of 8 cm × 8 cm × 8 cm. A pair of ZnSe observation windows (∅15 × 2 mm) are mounted parallel on the two opposite side walls for Fourier-transform infrared (FTIR) detection. Figure 1(a) shows a schematic of the PAW generation process. During the discharge, electrical and FTIR detections were performed, and four experimental groups with different discharge times were used: 2.5, 5, 7.5, and 10 min.

Figure 1(b) shows a schematic of the gas phase ammonia volatilization and aqueous-phase detection. The main aqueous-phase products of the PAW and their concentrations were measured and calculated through ultraviolet–visible (UV–Vis) absorption spectroscopy. The PAW after cooling in a sealed tube was then mixed with ammonia water with mass fractions of 0.15%, 0.25%, 0.5%, 1%, 5%, and 10% in a ratio of 9:1. 2 ml of the mixed solution was injected into a transparent acrylic container with inner dimensions of 19 cm × 14 cm × 33 cm with a pair of ZnSe window for free volatilization. The changes in volatilized NH_3 within 300 s were detected by an FTIR spectrometer. For the mixed solution, the concentrations of the main aqueous-phase products were also obtained by the UV–Vis method, while the pH and conductivity concentrations were measured using a multifunctional aqueous-phase measuring instrument. To analyze and compare the liquid detection results, [PAW/DIW] and [DIW/ammonia water] were mixed at a ratio of 9:1 respectively as controls. PAW-2.5, PAW-5, PAW-7.5, and PAW-10 represent PAWs with discharge times of 2.5, 5, 7.5, and 10 min, respectively. At least three experiments were carried out under each condition to reduce the influence of experimental error.

2.2. Measurement methods

To monitor the circuit parameters during discharging, a sampling resistor (10 Ω) was connected between the discharge device and the ground electrode. The voltage across the discharge and sampling resistor was measured using an oscilloscope DPO3034 (Tektronix, USA) equipped with

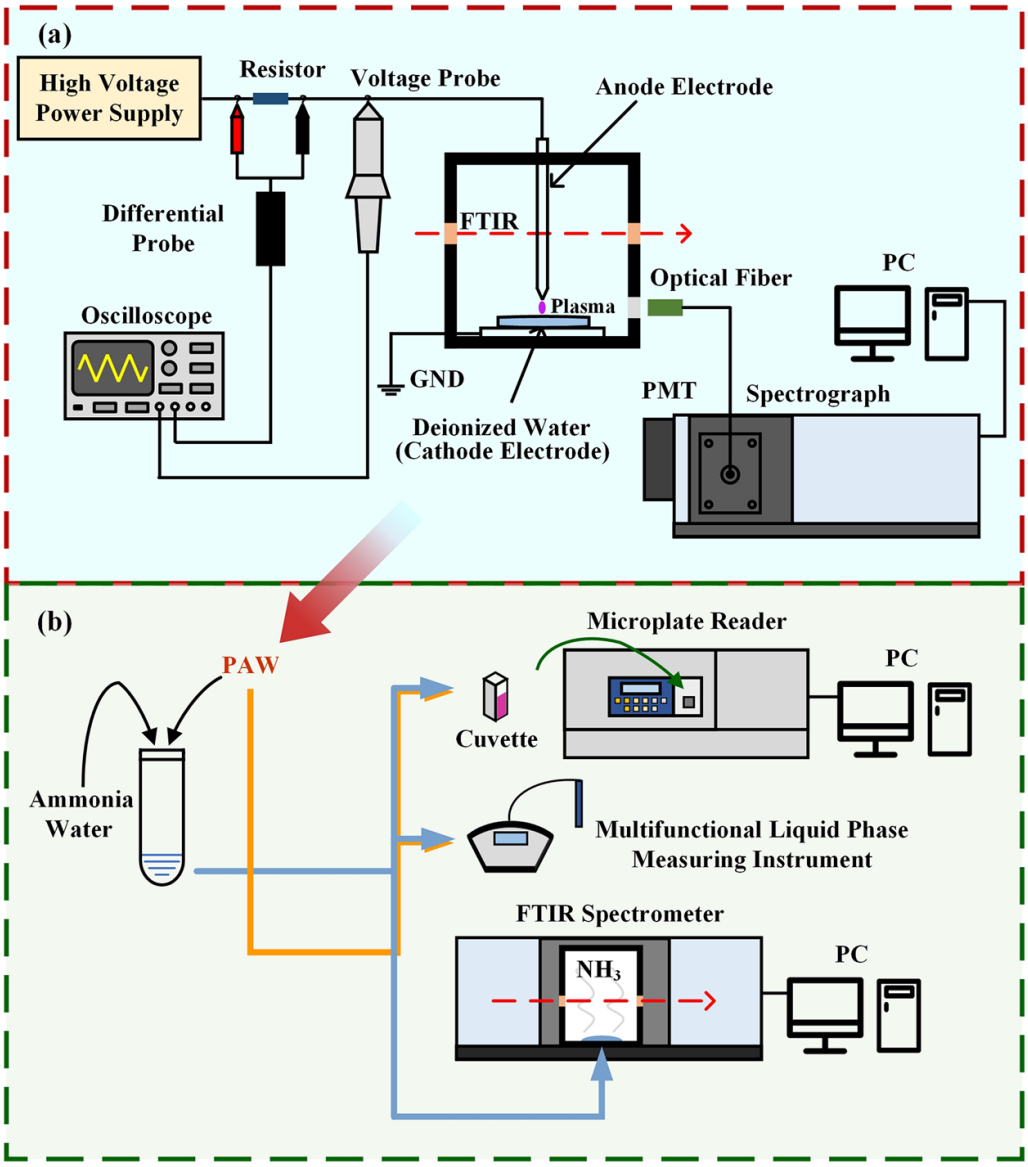

Figure 1. Schematic of the experiment setup. (a) Generation of PAW and (b) ammonia volatilization and detection.

a voltage probe P6015A (Tektronix, USA) and differential probe P5200A (Tektronix, USA), respectively. The discharge power could be calculated using the following equation [24]:

$$P = \frac{1}{T}\frac{1}{R}\int_0^T U_D U_R \mathrm{d}t \tag{1}$$

where P is the discharge power, T is the period of the discharge voltage, R is the sampling resistance connected to the circuit, U_D is the discharge voltage between the discharge electrode and ground electrode, and U_R is the voltage difference across the sampling resistance. The current I_D of the circuit was calculated by $I_D = U_R/R$.

During the generation of PAW and NH_3 volatilization from a mixed solution of PAW and ammonia water, FTIR detection was performed every 20 s using an FTIR spectrometer (Bruker, Vertex 70). This allowed for the identification of gas products and analysis of gas product concentration changes.

In this study, the concentration of volatilized NH_3 was quantitatively calculated. The IR of PAW against NH_3 volatilization was calculated using the formula:

$$IR = \left(1 - \frac{\overline{c_{PAW}}}{\overline{c_{DIW}}}\right) \times 100\%, \tag{2}$$

where $\overline{c_{PAW}}$ is the average concentration of NH_3 from the mixed solution of PAW and ammonia water at a given moment and $\overline{c_{DIW}}$ is from the mixed solution of DIW and ammonia water.

The UV–Vis absorption spectrum of reactive species in PAW was measured using a UV/Vis Microplate Spectrometer SpectraMax M4 (Molecular Devices, USA). The concentrations of NO_3^- and NO_2^- were determined using a chromogenic reaction and UV–vis spectroscopy [34–36]. Due to the limitations of the instrument's absorbance range and the linear chromogenic range of the chromogenic agent, the sample solution was diluted eight times.

For the measurement of NO_3^- concentration, a 2,6-dimethylphenol solution was prepared. 0.122 g of 2,6-dimethylphenol was dissolved in 100 ml of glacial acetic acid. In addition, 100 ml of a mixed acid solution of sulfuric acid and phosphoric acid in a ratio of 1:1 was prepared in advance and cooled to room temperature. To eliminate the influence of NO_2^- in the tested solution, 0.04 g of sulfamic acid was added to the mixed acid and thoroughly mixed. For detection, 1400 μl of the mixed acid, 200 μl of the tested solution, and 200 μl of 2, 6-dimethylphenol solution were mixed in a centrifuge tube and left for 10 min. The absorbance of the solution at 324 nm was then measured. By preparing $NaNO_3$ standard solutions with various concentration gradients ranging from 62.5 to 3000 μmol l^{-1} beforehand, a relationship curve between NO_3^- concentration and absorbance was obtained through experiments and fitting. Subsequently, the diluted sample solution could be measured, and the NO_3^- concentration of the sample solution could be calculated.

For the measurement of NO_2^- concentration, a self-configured chromogenic Griess reagent was used. A 0.861 g of sulfa, 0.259 g of N-(1-naphthyl) ethylenediamine dihydrochloride, and 1.5946 g of anhydrous citric acid were dissolved in 100 ml of methanol. For detection, 800 μl of Griess reagent and 800 μl of the solution being tested were mixed in a centrifuge tube at a ratio of 1:1 and left for 10 min. The absorbance at 523 nm was then measured. A $NaNO_2$ standard solution with multiple concentration gradients within the range of 0–250 μmol l^{-1} was used. By fitting the relationship curve between NO_2^- concentration and absorbance, the diluted sample solution could be measured, and the NO_2^- concentration could be calculated.

The pH and conductivity measurements were performed using the multifunctional liquid-phase measuring instrument MP551 (SANXIN, China). Before each test, the instrument was calibrated with pH and conductivity calibration solutions, respectively. The NO_3^- concentrations, NO_2^- concentrations, pH values, and conductivities of PAW and the mixed solution of PAW and ammonia water in each experimental group were quantitatively measured.

3. Results

We analyze the results mainly through plasma parameters, aqueous-phase product revolution of PAW, volatile NH_3 measurement from mixed solutions of PAW and ammonia water, and aqueous-phase product revolution of mixed solutions of PAW and ammonia water.

3.1. Air discharge and the products in the gas/aqueous phase

An image of the needle–water air discharge is shown in figure 2(a), and the typical voltage and current waveforms are shown in figure 2(b). Both the voltage and current exhibit irregular waveforms that change periodically. Throughout the discharge period, the discharge voltage U_D experiences a rapid increase from ∼460 V to ∼1675 V, followed by a gradual decrease. The current I_D follows a similar trend. The calculated discharge power is approximately 12.76 W.

The FTIR spectrum of gas-phase products during discharging is shown in figure 3. The prominent gas-phase products observed are NO_2 (at 1550–1675 cm^{-1}) and NO (at 1800–1950 cm^{-1}). Notably, the intensity of NO_2 increases as the discharge time progresses, as seen in the enlarged spectrum in figure 3(b). Simultaneously, a significant amount of OH (X) (at 3200–3600 cm^{-1}) is detected. During the discharge, water vapor molecules dissociate to produce •OH, leading to a gradual increase in OH(X) [37–41]. As the discharge continues, the water vapor will have significant impact on the FTIR measurement after 180 s.

As the revolution of aqueous-phase products of PAW, figure 4(a) shows the UV–Vis absorption spectrum acquired by the UV/Vis Microplate Spectrometer. The main components identified in PAW are NO_3^- (at 250–325 nm) and NO_2^- (at 325–400 nm). With increasing discharge time, the absorbance of NO_3^- gradually increases, while that of NO_2^- decreases. Figure 4(b) provides the concentrations of NO_3^- and NO_2^- in PAW for different discharge times. The concentration of NO_3^- increases from ∼5 mmol l^{-1} (PAW-2.5) to ∼19 mmol l^{-1} (PAW-10), whereas the NO_2^- concentration declines from ∼1.6 mmol l^{-1} (PAW-2.5) to ∼0.9 mmol l^{-1} (PAW-10). Furthermore, it is worth noting that the concentration of NO_3^- in PAW is significantly higher than that of NO_2^-. Figure 4(c) displays the pH and conductivity results of PAW. The pH gradually decreases from ∼2.21 (PAW-2.5) to ∼1.81 (PAW-10), while the conductivity rises from ∼1891 μS cm^{-1} (PAW-2.5) to ∼7027 μS cm^{-1} (PAW-10). The pH of DIW is ∼6.8, with a conductivity below 1 μS cm^{-1}.

3.2. The inhibition effect of NH_3 volatilization by PAW

Figure 5(a) shows a typical FTIR spectrum of the gas-phase products volatilized from the mixed solution of PAW-5 and 1% ammonia water. The spectrum exhibits a significant infrared absorption peak in the range of 900–1000 cm^{-1}, corresponding to NH_3. As the volatilization time increases, the absorbance of NH_3 gradually increases, indicating an increase in NH_3 concentration. To obtain quantitative results, the aforementioned procedure was repeated for all experimental groups and control groups (DIW mixed with ammonia water in a ratio of 9:1).

The calculated NH_3 concentration in the cavity is presented in figures 5(b)–(g). The volatile NH_3 concentration shows a gradual increase with volatilization time, and the results show that PAW has a considerable impact on the volatilization of NH_3 in the mixture of PAW and ammonia water. In the experimental groups with an ammonia concentration of no more than 1%, all groups can inhibit NH_3 volatilization. Among these groups, PAW-10 exhibits the strongest inhibitory effect. However, not all experimental groups can inhibit NH_3 volatilization; some experimental conditions even promote NH_3 volatilization. This phenomenon is particularly evident in the

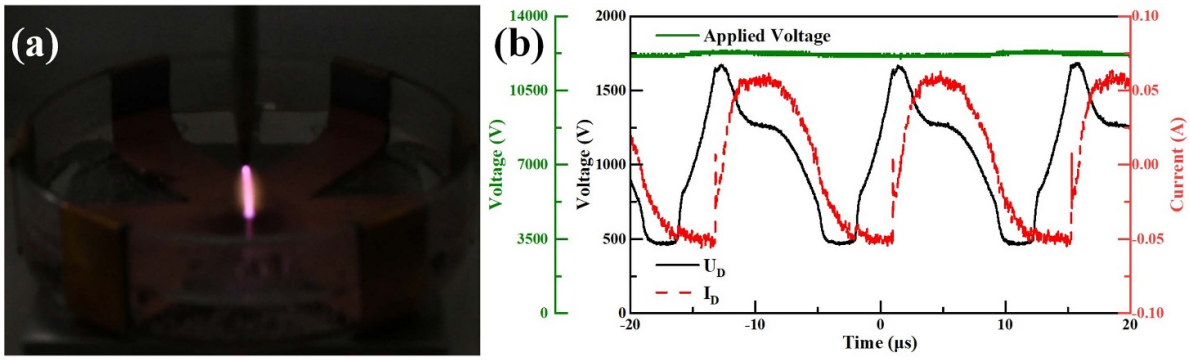

Figure 2. (a) Air discharge image; (b) voltage and current waveforms.

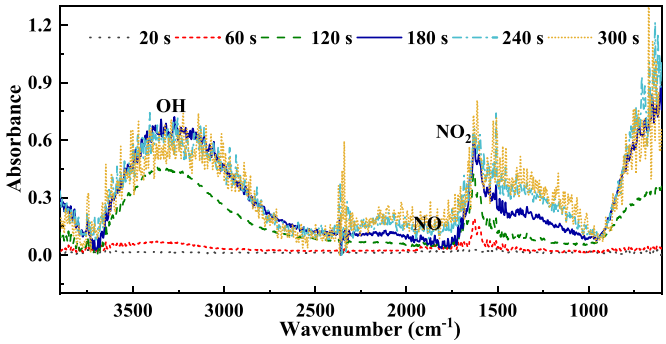

Figure 3. FTIR spectrum revolution of gas-phase products during discharging.

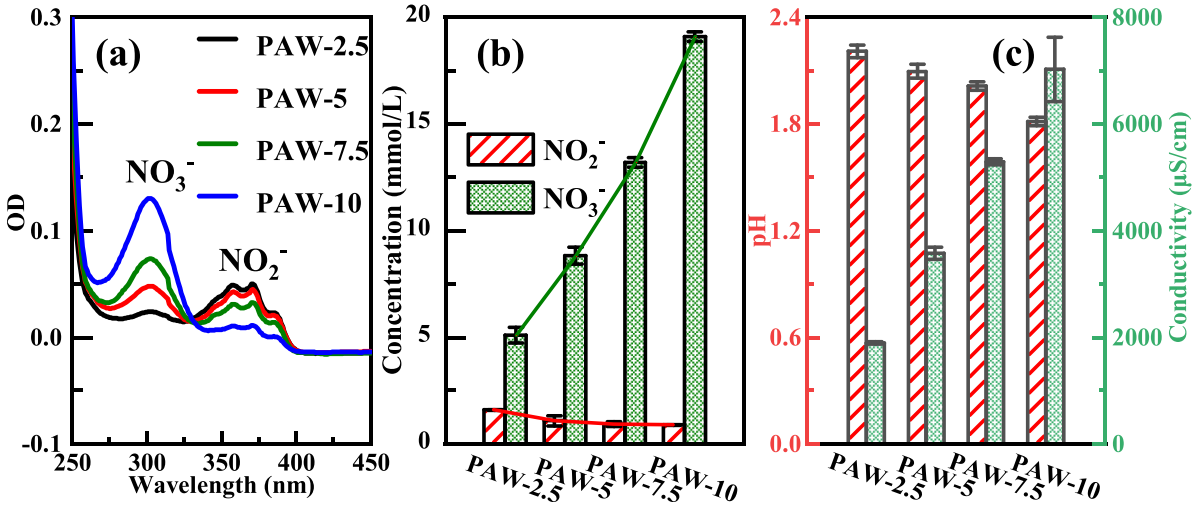

Figure 4. Revolution of aqueous-phase products of PAW. (a) UV–Vis spectrum, (b) NO_3^- and NO_2^- concentrations, and (c) pH and conductivity.

experimental groups with high concentrations of ammonia water, such as 5% and 10%. When the mass fraction is 10%, PAW-2.5, PAW-5, and PAW-7.5 promote NH_3 volatilization, while only PAW-10 consistently inhibits NH_3 volatilization.

To directly analyze the inhibition effect of PAW on NH_3 volatilization, we calculated the IR of each experimental group, as shown in figure 6. Figures 6(a)–(d) shows that the IR of NH_3 volatilization gradually increases with the discharge time of PAW. When PAWs with 0.25% ammonia are used, the IR reaches 100% after a discharge time of more than 5 min. Furthermore, when mixed with 0.15% ammonia water, the IR reaches 100% except for ∼77% of PAW-2.5. When the ammonia concentration is further reduced to 0.1% or lower, the IR could reach 100% in all cases. Conversely, when the ammonia water concentration is higher (figures 6(e) and (f)), the IR decreases upon mixing with PAW-2.5 to PAW-5. The inhibition effect of PAW-5 is the weakest for mixing with 5% and 10% ammonia waters, with IRs of −6% and −12% at 300 s,

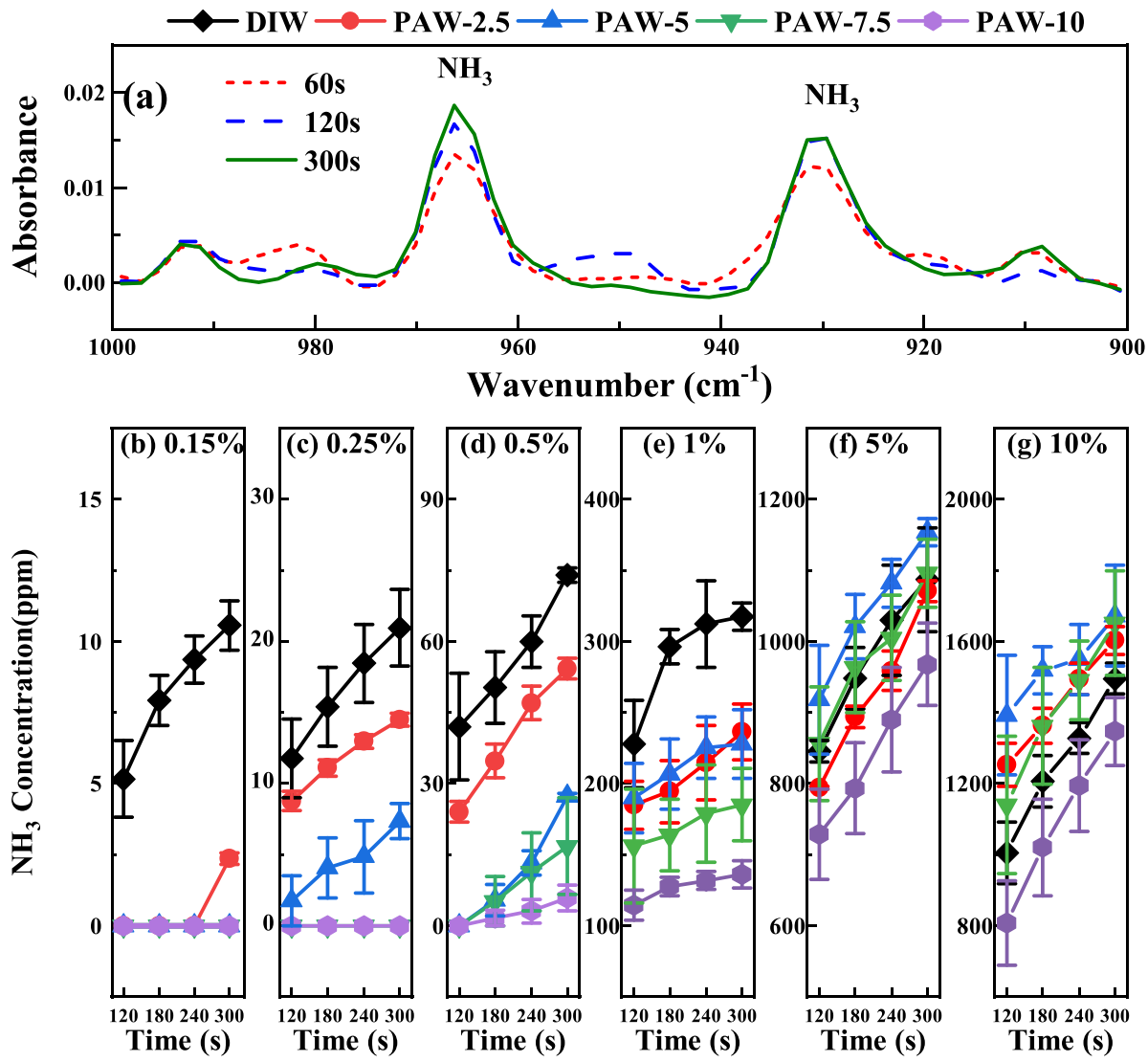

Figure 5. (a) Typical FTIR spectrum of the gas-phase products volatilized from PAW-5 mixed with 1% ammonia water, volatile NH_3 concentration from PAW mixed with ammonia water, where the mass fraction of ammonia water is (b) 0.15%, (c) 0.25%, (d) 0.5%, (e) 1%, (f) 5% and (g) 10%.

respectively, which considerably promotes NH_3 volatilization. For mixing with PAW-10, the IR increased to ∼11% and ∼10%, respectively. Moreover, for the experimental groups with different ammonia water concentrations, at the same discharge time, the IR gradually decreased with the increase in ammonia water concentration. For example, the IR of PAW-10 at 300 s decreased from ∼100% to ∼10%, while the IR of PAW-5 decreased from ∼65% to ∼−12%.

Therefore, the discharge time of PAW and ammonia water concentration have significant effects on the inhibition effect. The promotion of NH_3 volatilization under some experimental conditions may attribute to the large amount of heat released from the neutralization reaction between acidic PAW and ammonia water which largely enhanced the NH_3 volatilization and overcome the inhibition effect.

3.3. Aqueous-phase product revolution of the PAW mixed with ammonia water

Concentrations of components in the mixed solution are compared in figure 7. Figure 7(a) shows the concentrations of NO_3^- in different mixed groups. The concentration of NO_3^- remains relatively constant in the mixed solution when ammonia water with different concentrations or DIW is mixed with a PAW solution with a fixed discharge time. However, when the concentration of ammonia water is fixed, the NO_3^- concentration in the mixed solution increases with the discharge time. For example, for PAW mixed with 1% ammonia water, the NO_3^- concentration increases from ∼4.60 mmol l^{-1} (PAW-2.5) to ∼17.8 mmol l^{-1} (PAW-10).

Figure 7(b) shows the concentrations of NO_2^-. The concentration of NO_2^- in the mixed solution decreases with the

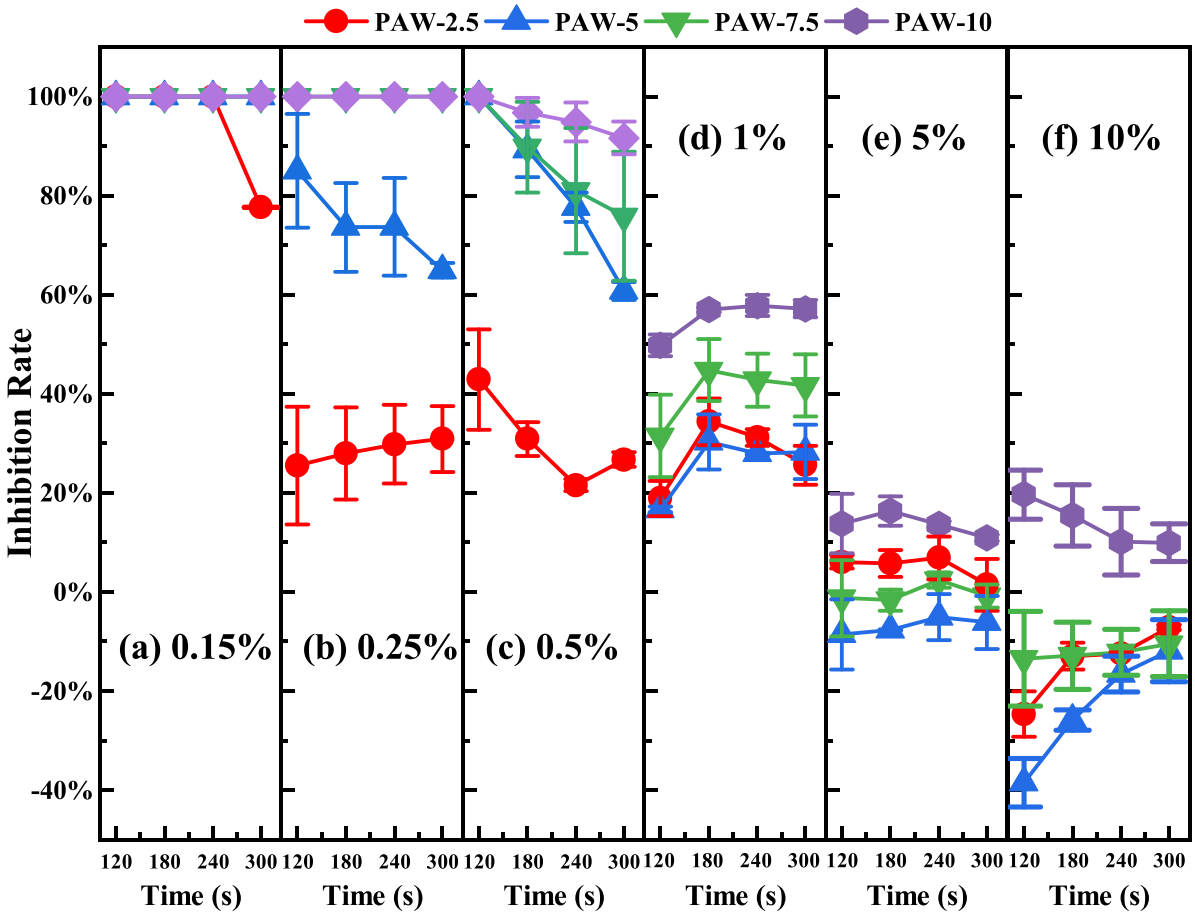

Figure 6. IR of NH_3 volatilization, where the mass fraction of ammonia water is (a) 0.15%, (b) 0.25%, (c) 0.5%, (d) 1%, (e) 5%, and (f) 10%.

increase in the ammonia water concentration as well as the discharge time. For example, the concentration of NO_2^- in all experimental groups of PAW-10 gradually decreases from ∼0.84 mmol l^{-1} for PAW mixed with DIW to ∼0.29 mmol l^{-1} for PAW mixed with 10% ammonia water.

Figure 8(a) shows pH changes in different groups. When PAW is mixed with DIW or ammonia water of varying concentrations, the pH of the mixed solution decreases as the discharge time of PAW increases. The mixed solution with DIW is acidic, with a decrease in pH from ∼2.57 (PAW-2.5) to ∼1.90 (PAW-10). Most other mixed solutions are alkaline, exhibiting lower pH values compared to the mixed solution of the same ammonia water and DIW. When PAW with the same discharge time is mixed with ammonia water, the pH gradually increases with the increase in ammonia water concentration. As the concentration of ammonia water decreases and the discharge time of PAW increases, the pH of the mixed solution tends to become acidic. For instance, when mixing 0.15% ammonia water with PAW-7.5 or PAW-10, or when mixing 0.25% ammonia water with PAW-10, the resulting solution becomes acidic, and the IR is ∼100%.

Figure 8(b) shows the results of conductivity changes. When PAW is mixed with DIW or ammonia water of varying concentrations, the conductivity of the mixed solution increases with the discharge time of PAW. For instance, in groups where PAW is mixed with 1% ammonia water, the conductivity increases from ∼855 μS cm^{-1} (PAW-2.5) to ∼2553 μS cm^{-1} (PAW-10), indicating the generation of more active particles in PAW. The conductivity of PAW mixed with ammonia water is significantly lower than that of PAW mixed with DIW, primarily due to the more substantial contribution of H^+ in PAW to the overall conductivity, compared to other ions. This also explains the slight increase in conductivity observed in slightly acidic mixed solutions. Furthermore, the conductivity of PAW mixed with different concentrations of ammonia water is higher than that of DIW mixed with ammonia water. This observation suggests that the mixing of PAW with ammonia water introduces a greater number of active ions into the ammonia water. This can be attributed to the addition of NO_3^- and NO_2^- ions from PAW, as well as the conversion of $NH_3{\cdot}H_2O$ or NH_3 molecules in the ammonia water into NH_4^+. The conversion of $NH_3{\cdot}H_2O$ or NH_3 to NH_4^+ helps reduce NH_3 volatilization and enhances the absorption and utilization of nitrogen elements by crops when used as a fertilizer. Moreover, when PAW is mixed with ammonia water for the same discharge time, its conductivity gradually increases with the concentration of ammonia water.

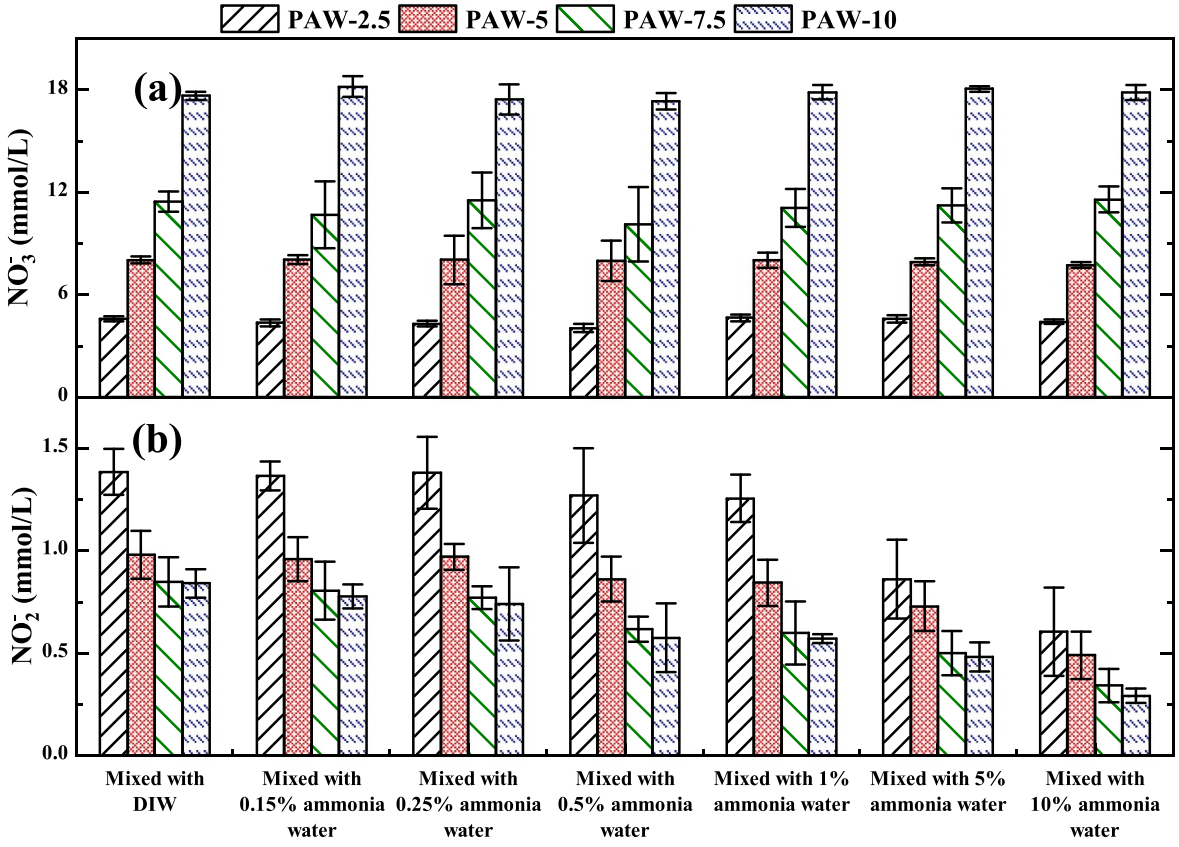

Figure 7. Concentration comparison of solution components: (a) NO_3^- and (b) NO_2.

4. Discussion

Existing studies on the interaction between plasma and animal slurry or other fertilizers mainly focus on the direct use of gas plasma to treat fertilizer, creating a plasma-activated organic fertilizer [42, 43], which is still at the initial stage and requires further studies to determine its feasibility. The limited research only conducted partial field trials to verify the enhanced effectiveness of nitrogen fertilizer other than the ability to inhibit ammonia volatilization [42], nor the basic reaction processes. In this study, we proposed the use of air PAW to inhibit NH_3 volatilization from agriculture and livestock and achieved a detailed analysis of the basic process of plasma indirect treatment by detecting changes in gas-phase and liquid-phase components. The inhibition effect of PAW is directly related to the concentrations of H^+ and RONS, further related to the gas and liquid products [42]. The main reactions involved in the air PAW generation are [15, 17, 22]:

$$e + N_2 \rightarrow N + \cdot N + e, \tag{3}$$

$$e + O_2 \rightarrow O + \cdot O + e, \tag{4}$$

$$H_2O + e \rightarrow \cdot OH + \cdot H + e, \tag{5}$$

$$H_2O + e \rightarrow \cdot OH + H^+ + 2e, \tag{6}$$

$$N + O \rightarrow NO, \tag{7}$$

$$N + O_2 \rightarrow NO + O, \tag{8}$$

$$N_2 + O \rightarrow NO + N, \tag{9}$$

$$NO + O \rightarrow NO_2, \tag{10}$$

$$2NO + O_2 \rightarrow 2NO_2, \tag{11}$$

$$NO + \cdot OH \rightarrow HNO_2, \tag{12}$$

$$NO_2 + \cdot OH \rightarrow HNO_3, \tag{13}$$

$$2NO_2 + H_2O \rightarrow NO_2^- + NO_3^- + 2H^+, \tag{14}$$

$$NO + NO_2 + H_2O \rightarrow 2NO_2^- + 2H^+ \ . \tag{15}$$

During the discharge process, the gas-phase products such as NO_2 and NO are not fully dissolved in the solution. Improving the generation efficiency of PAW to ensure the production and absorption of more active particles in a shorter

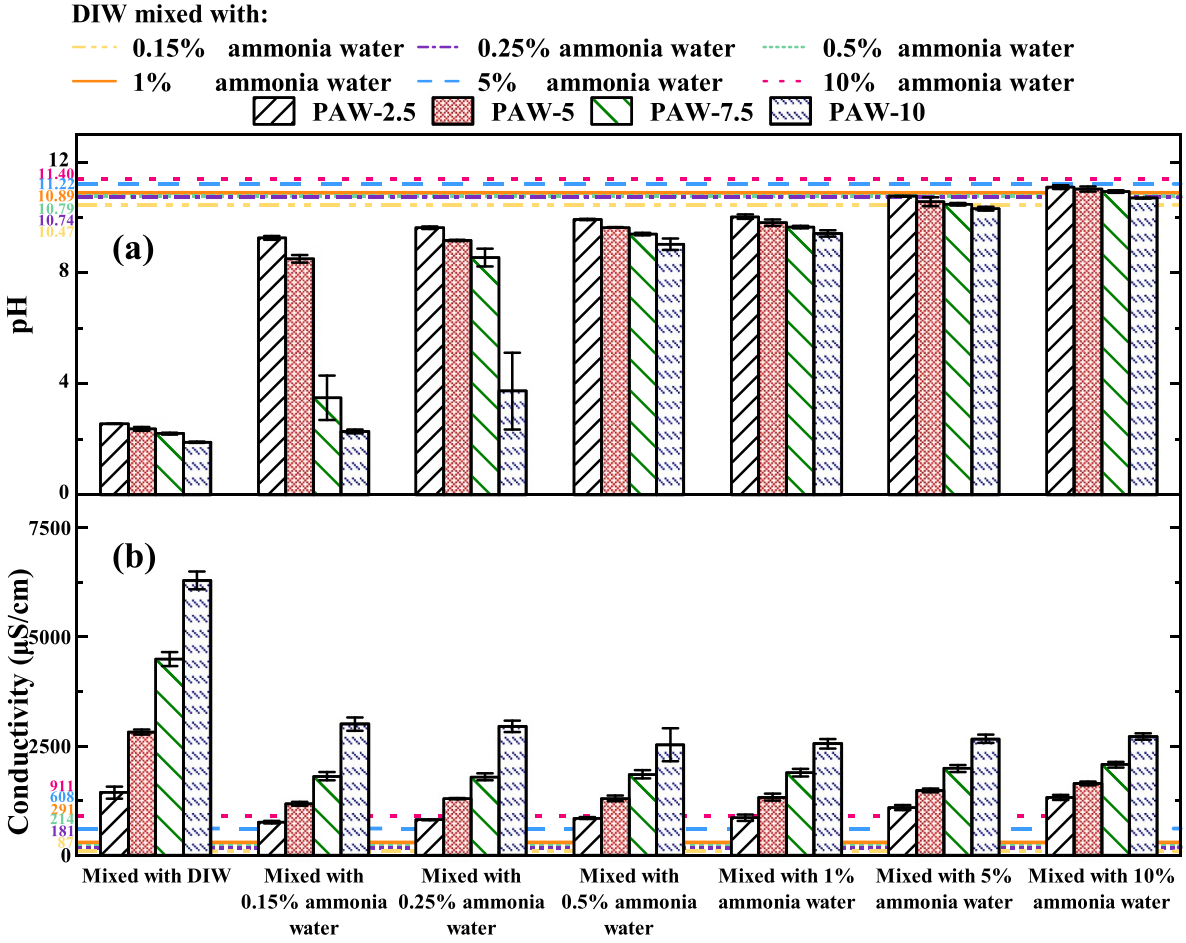

Figure 8. Comparison of the solution (a) pH values and (b) conductivities.

time is a key issue. Previous studies have shown that various factors, such as electrode configuration, plasma treatment time, applied voltage, gas environment, solution composition and volume, as well as treatment method, have significant impacts on the generation of RONS and the physicochemical properties (pH and conductivity) of PAW [15, 22, 44, 45]. By combining with plasma bubbling technology, it is possible to further improve the energy efficiency in our system. For example, the application of plasma bubbling can enhance the absorption efficiency by increasing the interaction between plasma reactive species and the solution, while reducing the loss of plasma reactive species. Various techniques have been explored in the existing literatures, including plasma-bubble column reactors, underwater bubbling discharge, and nanosecond pulse microbubble plasma reactors [46–49]. Alternatively, we can also improve the production efficiency of PAW by improving the plasma source to convert the current main reaction products, NO and NO_2, into N_2O_5, which exhibits higher solubility and activation efficiency [50–52]. These devices could be operated in series to further enhance the production efficiency of PAW.

As shown in section 3.2, the long-term stable components of PAW in this experiment are mainly NO_3^-, NO_2^-, and H^+. With the increase in the discharge time, more active particles are generated, the pH of the solution goes down, and more NO_2^- are oxidized to NO_3^- [17]. As ammonia water is used as an ammonia source in this experiment to simulate the volatilization of NH_3, the main influencing factors should be the pH, ammonia water concentration, and temperature [53–55]. Among them, the temperature of ammonia water and PAW is constant, but the heat released through the mixing of ammonia water and PAW may have a certain influence on the temperature. As mentioned in section 3.2, both the discharge time of the PAW and the concentration of ammonia have significant influences on the inhibitory effect. We speculate that the emersion of the promoting effect is related to the release of more heat during the neutralization reaction between the acidic PAW with ammonia water. This is further influenced by PAW pH and ammonia water concentration. According to section 3.3, the pH of the PAW is inversely proportional to the change in the discharge time, and a lower pH inhibits NH_3 volatilization. A higher mass fraction of ammonia water promotes NH_3 volatilization. In summary, the IR is related to the pH of the PAW and the concentration of ammonia water. The main reactions in this process are:

$$NH_4^+ + OH^- \leftrightarrow NH_3 \cdot H_2O \rightarrow NH_3 \uparrow + H_2O, \qquad (16)$$

$$NH_3 \cdot H_2O + H^+ \rightarrow NH_4^+ + H_2O, \quad (17)$$

$$H^+ + OH^- \rightarrow H_2O \ . \quad (18)$$

When the pH of the PAW is low, it promotes a shift of the equation (16) to the left and inhibits the NH_3 volatilization. When the mass fraction of ammonia water is very high, it promotes a shift of the equation (16) to the right and larger NH_3 volatilization.

After the PAW is mixed with ammonia water, more NO_x^- are introduced into the ammonia water, and more NH_3 and $NH_3{\cdot}H_2O$ are converted to NH_4^+, resulting in the addition of more active nitrogen elements and improving fertility. Compared to PAW mixed with DIW, the NO_3^- concentration is almost unchanged, while the NO_2^- concentration decreases, likely as HNO_2 and NO_2^- react with ammonia water to form NH_4NO_2, which can easily decompose. Particularly, when PAW is mixed with ammonia water, it releases heat and promotes the decomposition of a part of NH_4NO_2 into N_2 and H_2O [56, 57]:

$$HNO_2 + NH_3 \cdot H_2O \rightarrow NH_4NO_2 + H_2O, \quad (19)$$

$$NH_4^+ + NO_2^- \rightarrow NH_4NO_2, \quad (20)$$

$$NH_4NO_2 \rightarrow N_2 \uparrow + 2H_2O \ . \quad (21)$$

When the ammonia water concentration is higher, more HNO_2 and NO_2^- are involved in the reaction, and thus the decomposition of NH_4NO_2 is larger. This also explains the slight decrease in the NO_2^- concentration with the increase in the ammonia water concentration. However, as the NO_2^- concentration is relatively low compared to that of NO_3^-, the N loss from this reaction could be ignored. To avoid this N loss, during the PAW generation process, NO_2^- could be transformed into NO_3^- with the increase in the rest time [58].

To further verify the effect of the pH of the final mixed solution on the IR of NH_3 volatilization, we established a regression model to the pH of the mixed solution with the IR at 300 s. The model is

$$IR = -6.331 + \frac{106.331}{1+\left(\frac{pH_{MIX}}{9.630}\right)^{34.679}}, \quad (22)$$

where IR (%) is the IR of ammonia volatilization and pH_{MIX} is the pH of the mixed solution of PAW and ammonia water. The adjusted goodness of fit ${R_1}^2$ is 0.940 96, which is closer to 1. Considering the errors in the calculation and detection methods, the goodness of fit of this model is satisfactory.

The effect of the pH of the mixed solution on the ammonia water volatilization is shown in figure 9. It can be seen that the IR closely relates to the pH value of the PAW and ammonia water mixture. The IR basically decreases with the increase of the pH value. After controlling the pH value within a certain range (approximately below 8), the IR can achieve IRs that are very close to 100%. However, when the pH value of the mixture is over 10.5, the NH_3 volatilization promotion will happen.

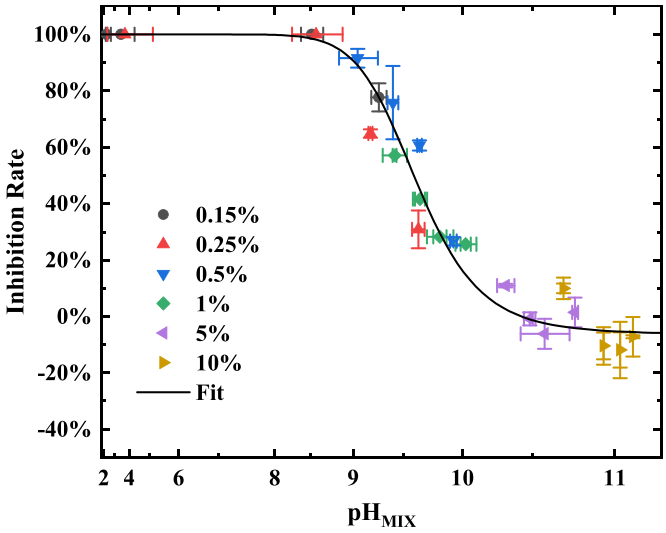

Figure 9. Effect of the pH of the PAW mixed with ammonia water on the ammonia water volatilization.

The acidification of animal urine or liquid fertilizers by PAW can also add an N element to the fertilizers to improve its value as a nitrogen fertilizer, meanwhile, the use of air plasma for slurry treatment may reduce the concentration of organic compounds that cause odor (such as skatole ('fecal odor') and p-cresol ('pig odor')), while also decreasing the bacterial loads [42, 43]. There are currently limited researches on using plasma directly to suppress ammonia volatilization in slurry [42, 43] or using indirect plasma treatment as that in our research. The method of using plasma direct treatment did not conduct a detailed analysis of its basic process, nor did it focus on the component changes and action mechanisms during the reaction process. Only partial field trials were conducted to verify the effectiveness of NH_3 inhibition. However, the development of PAW is relatively mature, especially compared to using discharge plasma to directly treat the animal slurry. PAW is not a simple acid, and studying its chemical process is of great importance. This paper achieves a detailed analysis of the basic process of plasma indirect treatment by detecting changes in gas-phase and liquid-phase components.

The industrial synthesis of HNO_3 predominantly employs the ammonia oxidation route, a pivotal process commencing with the catalytic conversion of NH_3 into NO at elevated temperatures (~760 °C–840 °C) using a Pt–Rh catalyst. This is succeeded by the sequential oxidation of NO to NO_2 and ultimately, NO_2 interacts with water in an absorption tower to produce HNO_3. The energy consumption throughout this multipart process includes energy-intensive stages like gas compression, substantial heating for oxidation reactions, cooling during the absorption phase, and the maintenance of recycling systems. In addition, the reaction raw material of the above process is NH_3, and the synthetic NH_3 industry itself will consume a lot of energy, whose theoretical energy consumption (H–B method, ~34 GJ tN^{-1}) [59] is ~2.5 times higher than the theoretical energy consumption of low-temperature plasma

nitrogen fixation (∼14 GJ tN^{-1}) [60]. Although there is still a certain gap between the actual energy consumption of low temperature plasma for nitrogen fixation and the theoretical value, with the development of plasma technology, this gap will be gradually reduced. For example, using different discharge structures could largely lower the energy cost on NO_x production, such as propeller arc discharge (∼250 GJ tN^{-1}), glow discharge with the magnetic field (∼189 GJ tN^{-1}), rotating arc (∼48 GJ tN^{-1}), etc [61–64], which will further improve the energy efficiency of PAW production. In addition, compared to the industry method of producing HNO_3, the main advantages of using PAW for processing slurry lie in the convenient and environmentally friendly nature of PAW preparation, as well as the abundant and easily obtainable raw materials (water and air). Meanwhile, the PAW production process emits fewer pollutants. On the other hand, transporting acid to remote agricultural and pastoral areas involves safety security cost and transportation cost issues. Compared to the direct use of nitric acid or other acid solutions, PAW can be easily prepared and controlled, and the requirements for the production system are smart and low-cost with raw materials consisting only of water and air. Therefore, PAW can be prepared on the spot in the application scene with small-scale production, ready to use with reduced transportation and storage costs. By utilizing abundant solar or wind energy resources in agriculture or livestock, PAW can significantly reduce production costs.

Besides, we have already proposed a new strategy to capture volatilized NH_3 by gas phase plasma products (mainly NO_x) [24, 25] to form solid NH_4NO_3 for N recycling in our previous study. The scheme proposed in this paper focuses on directly treating the volatile ammonia source with aqueous PAW, to inhibit the NH_3 volatilization, and adding more N elements into the source to improve fertility. By combination of these two strategies, the undissolved NO_x from the PAW generation stage can be used for NH_2 capture in the gas phase, thereby the N element in the form of NH_3 can be further reserved and recycled instead of losing into the atmosphere, which enhances the resource efficiency and mitigates the atmospheric pollution through reduced NH_3 emission and effective N recycling, especially in agricultural ammonia management.

5. Conclusion

The N loss from agriculture and livestock in the form of NH_3 is the main way in nitrogen cycle, which results in significant resource waste and environmental pollution. In this study, we proposed and evaluated the inhibition effect of air PAW on NH_3 volatilization. The discharge time of the PAW and the concentration of the ammonia water significantly affected the NH_3 volatilization. The effect of the discharge time was mainly due to the generation of more active particles and lower PAW pH at a longer discharge time. When a PAW with a discharge time of 5 min, 7.5 min or 10 min was mixed with ammonia water with a mass fraction of 0.15%, or PAW of 7.5 min or 10 min with 0.25% ammonia water, the IR reached ∼100%. The IR closely related to the pH value of the PAW and ammonia water mixture and basically decreased with the increase of the pH value. However, for ammonia water with a higher concentration, the effect of heat release for NH_3 volatilization when PAW was mixed with ammonia water may overcome the inhibition effect and led to NH_3 volatilization promotion. It is important to evaluate different concentrations of ammonia water to determine an appropriate PAW discharge time range. The regression model between the pH of the mixed solution and IR established by the experimental results in this study provides reference for the experimental analysis and condition determination.

Data availability statement

All data that support the findings of this study are included within the article (and any supplementary files).

Acknowledgments

This work is supported by the National Natural Science Foundation of China (No. 52177145).

ORCID iD

Zilan Xiong https://orcid.org/0000-0003-1095-3959

References

[1] Ertl G 1983 Primary steps in catalytic synthesis of ammonia *J. Vac. Sci. Technol.* A **1** 1247–53
[2] Humphreys J, Lan R and Tao S 2021 Development and recent progress on ammonia synthesis catalysts for Haber–Bosch process *Adv. Energy Sustain. Res.* **2** 14415–53
[3] Andrews M, Lea P J, Raven J A and Azevedo R A 2009 Nitrogen use efficiency. 3. Nitrogen fixation: genes and costs *Ann. Appl. Biol.* **155** 1–13
[4] Lassaletta L, Billen G, Grizzetti B, Anglade J and Garnier J 2014 50 year trends in nitrogen use efficiency of world cropping systems: the relationship between yield and nitrogen input to cropland *Environ. Res. Lett.* **9** 105011
[5] Omara P, Aula L, Oyebiyi F and Raun W R 2019 World cereal nitrogen use efficiency trends: review and current knowledge *Agrosyst. Geosci. Environ.* **2** 1–8
[6] Houlton B Z, Sigman D M and Hedin L O 2006 Isotopic evidence for large gaseous nitrogen losses from tropical rainforests *Proc. Natl Acad. Sci.* **103** 8745–50
[7] Fowler D *et al* 2013 The global nitrogen cycle in the twenty-first century *Phil. Trans. R. Soc.* B **368** 20130164
[8] Fowler D *et al* 2015 Effects of global change during the 21st century on the nitrogen cycle *Atmos. Chem. Phys.* **15** 13849–93
[9] Sutton M A *et al* 2013 Towards a climate-dependent paradigm of ammonia emission and deposition *Phil. Trans. R. Soc.* B **368** 20130166
[10] Bouwman L, Goldewijk K K, Van Der Hoek K W, Beusen A H W, Van Vuuren D P, Willems J, Rufino M C and Stehfest E 2013 Exploring global changes in nitrogen and phosphorus cycles in agriculture induced by livestock production over the 1900–2050 period *Proc. Natl Acad. Sci.* **110** 20882–7

[11] Fangueiro D, Hjorth M and Gioelli F 2015 Acidification of animal slurry—a review *J. Environ. Manage.* **149** 46–56
[12] Ahmed O H, Braine Yap C H and Nik Muhamad A M 2010 Minimizing ammonia loss from urea through mixing with zeolite and acid sulphate soil *Int. J. Phys. Sci.* **5** 2198–202
[13] Bourdin F, Sakrabani R, Kibblewhite M G and Lanigan G J 2014 Effect of slurry dry matter content, application technique and timing on emissions of ammonia and greenhouse gas from cattle slurry applied to grassland soils in Ireland *Agric. Ecosyst. Environ.* **188** 122–33
[14] Bruggeman P J *et al* 2016 Plasma–liquid interactions: a review and roadmap *Plasma Sources Sci. Technol.* **25** 053002
[15] Brisset J-L and Pawlat J 2016 Chemical effects of air plasma species on aqueous solutes in direct and delayed exposure modes: discharge, post-discharge and plasma activated water *Plasma Chem. Plasma Process.* **36** 355–81
[16] Rezaei F, Vanraes P, Nikiforov A, Morent R and De Geyter N 2019 Applications of plasma-liquid systems: a review *Materials* **12** 2751
[17] Thirumdas R, Kothakota A, Annapure U, Siliveru K, Blundell R, Gatt R and Valdramidis V P 2018 Plasma activated water (PAW): chemistry, physico-chemical properties, applications in food and agriculture *Trends Food Sci. Technol.* **77** 21–31
[18] Ranieri P, Sponsel N, Kizer J, Rojas-Pierce M, Hernández R, Gatiboni L, Grunden A and Stapelmann K 2021 Plasma agriculture: review from the perspective of the plant and its ecosystem *Plasma Process. Polym.* **18** 2000162
[19] Domonkos M, Tichá P, Trejbal J and Demo P 2021 Applications of cold atmospheric pressure plasma technology in medicine, agriculture and food industry *Appl. Sci.* **11** 4809
[20] Ito M, Ohta T and Hori M 2012 Plasma agriculture *J. Korean Phys. Soc.* **60** 937–43
[21] Bradu C, Kutasi K, Magureanu M, Puač N and Živković S 2020 Reactive nitrogen species in plasma-activated water: generation, chemistry and application in agriculture *J. Phys. D: Appl. Phys.* **53** 223001
[22] Zhou R, Zhou R, Wang P, Xian Y, Mai-Prochnow A, Lu X, Cullen P J, Ostrikov K (Ken) and Bazaka K 2020 Plasma-activated water: generation, origin of reactive species and biological applications *J. Phys. D: Appl. Phys.* **53** 303001
[23] Liu K, Ren W, Ran C, Zhou R, Tang W, Zhou R, Yang Z and Ostrikov K (Ken) 2021 Long-lived species in plasma-activated water generated by an AC multi-needle-to-water discharge: effects of gas flow on chemical reactions *J. Phys. D: Appl. Phys.* **54** 065201
[24] Zhu Y, Xiong Z, Li M, Chen X, Lu C and Zou Z 2021 Investigation of NH_4NO_3 formation by air plasma and wasted ammonia *Plasma Process. Polym.* **18** 2000223
[25] Li M, Hou Z, Dai Y, Song Z and Xiong Z 2023 Capture of NH_3 using air plasmas to form NH_4NO_3 for N recycling: impact factors and mechanisms *J. Clean. Prod.* **428** 139434
[26] Laubach J, Taghizadeh-Toosi A, Gibbs S J, Sherlock R R, Kelliher F M and Grover S P P 2013 Ammonia emissions from cattle urine and dung excreted on pasture *Biogeosciences* **10** 327–38
[27] Petersen S O, Sommer S G, Aaes O and Søegaard K 1998 Ammonia losses from urine and dung of grazing cattle: effect of N intake *Atmos. Environ.* **32** 295–300
[28] Zhang J, Giannis A, Chang V W C, Ng B J H and Wang J-Y 2013 Adaptation of urine source separation in tropical cities: process optimization and odor mitigation *J. Air Waste Manage. Assoc.* **63** 472–81
[29] Sherlock R and Goh K 1985 Dynamics of ammonia volatilization from simulated urine patches and aqueous urea applied to pasture. II. Theoretical derivation of a simplified model *Ferti Res.* **6** 3–22
[30] Liu B, Giannis A, Zhang J, Chang V W C and Wang J Y 2013 Characterization of induced struvite formation from source-separated urine using seawater and brine as magnesium sources *Chemosphere* **93** 2738–47
[31] Andrews W B 1956 Anhydrous ammonia as a nitrogenous fertilizer *Adv. Agron.* **8** 61–125
[32] Denmead O T, Freney J R and Simpson J R 1982 Atmospheric dispersion of ammonia during application of anhydrous ammonia fertilizer *J. Environ. Qual.* **11** 568–72
[33] Widdowson F V, Penny A and Flint R C 1972 Results from barley experiments comparing aqueous ammonia and aqueous urea with ammonium nitrate, and also liquid with granular NPK fertilizers *J. Agric. Sci.* **79** 349–61
[34] Sah R N 1994 Nitrate-nitrogen determination—a critical review *Commun. Soil Sci. Plant. Anal.* **25** 2841–69
[35] García-Robledo E, Corzo A and Papaspyrou S 2014 A fast and direct spectrophotometric method for the sequential determination of nitrate and nitrite at low concentrations in small volumes *Mar. Chem.* **162** 30–36
[36] Oh J-S, Szili E J, Ogawa K, Short R D, Ito M, Furuta H and Hatta A 2018 UV–vis spectroscopy study of plasma-activated water: dependence of the chemical composition on plasma exposure time and treatment distance *Jpn. J. Appl. Phys.* **57** 0102B9
[37] Kusumandari K, Saraswati T E, Wulandari S W and Qusnudin A 2022 Atmospheric air plasma corona discharge for dye degradation of Indonesian batik wastewater *Indian J. Phys.* **96** 1001–8
[38] Dimpfl W L and Kinsey J L 1979 Radiative lifetimes of OH(A2Σ) and Einstein coefficients for the A-X system of OH and OD *J. Quant. Spectrosc. Radiat. Transfer* **21** 233–41
[39] Wang C and Wu W 2014 Roles of the state-resolved OH(A) and OH(X) radicals in microwave plasma assisted combustion of premixed methane/air: an exploratory study *Combust. Flame* **161** 2073–84
[40] Sun M and Cai L J 2012 Diagnosis of OH radicals in air negative pulsed discharge with nozzle-cylinder electrode by optical emission spectroscopy *IEEE Trans. Plasma Sci.* **40** 1395–8
[41] Roy N C, Talukder M R and Chowdhury A N 2017 OH and O radicals production in atmospheric pressure air/Ar/H_2O gliding arc discharge plasma jet *Plasma Sci. Technol.* **19** 125402
[42] Graves D B, Bakken L B, Jensen M B and Ingels R 2019 Plasma activated organic fertilizer *Plasma Chem. Plasma Process.* **39** 1–19
[43] Ingels R and Graves D B 2015 Improving the efficiency of organic fertilizer and nitrogen use via air plasma and distributed renewable energy *Plasma Med.* **5** 257–70
[44] Rathore V and Nema S K 2021 Optimization of process parameters to generate plasma activated water and study of physicochemical properties of plasma activated solutions at optimum condition *J. Appl. Phys.* **129** 084901
[45] Gott R P, Engeling K W, Olson J and Franco C 2023 Plasma activated water: a study of gas type, electrode material, and power supply selection and the impact on the final frontier *Phys. Chem. Chem. Phys.* **25** 5130–45
[46] Rathore V, Jamnapara N I and Nema S K 2023 Enhancing the physicochemical properties and reactive species concentration of plasma activated water using an air bubble diffuser *Phys. Lett.* A **482** 129035
[47] Man C, Zhang C, Fang H, Zhou R, Huang B, Xu Y, Zhang X and Shao T 2022 Nanosecond-pulsed microbubble plasma reactor for plasma-activated water generation and bacterial inactivation *Plasma Process. Polym.* **19** e2200004
[48] Wu M-C, Uehara S, Wu J-S, Xiao Y, Nakajima T and Sato T 2020 Dissolution enhancement of reactive chemical species

by plasma-activated microbubbles jet in water *J. Phys. D: Appl. Phys.* **53** 485201
[49] Han J-Y, Park S-H and Kang D-H 2023 Effects of plasma bubble-activated water on the inactivation against foodborne pathogens on tomatoes and its wash water *Food Control* **144** 109381
[50] Sasaki S, Takashima K and Kaneko T 2021 Portable plasma device for electric N_2O_5 production from air *Ind. Eng. Chem. Res.* **60** 798–801
[51] Wang Z *et al* 2022 Combination of NO_x mode and O_3 mode air discharges for water activation to produce a potent disinfectant *Plasma Sources Sci. Technol.* **31** 05LT01
[52] Wang Z, Zhu M, Liu D, Liu L, Wang X, Chen J, Guo L, Liu Y, Hou M and Rong M 2023 N_2O_5 in air discharge plasma: energy-efficient production, maintenance factors and sterilization effects *J. Phys. D: Appl. Phys.* **56** 075204
[53] Wang W L, Liu B, Han R M, Wang Y, Liu X, Xu Q, Li W J and Tang X Y 2016 Review of researches on factors affecting emission of ammonia from agriculture *J. Ecol. Rural Environ.* **32** 870–8
[54] Ju X and ZHANG C 2017 Nitrogen cycling and environmental impacts in upland agricultural soils in North China: a review *J. Integr. Agric.* **16** 2848–62
[55] Ernst J W and Massey H F 1960 The effects of several factors on volatilization of ammonia formed from urea in the soil *Soil Sci. Soc. Am. J.* **24** 87–90
[56] Hao R, Mao Y, Mao X, Wang Z, Gong Y, Zhang Z and Zhao Y 2019 Cooperative removal of SO_2 and NO by using a method of UV-heat/H_2O_2 oxidation combined with NH_4OH-$(NH_4)_2SO_3$ dual-area absorption *Chem. Eng. J.* **365** 282–90
[57] Li M, Yeom Y, Weitz E and Sachtler W M H 2006 An acid catalyzed step in the catalytic reduction of NO_x to N_2 *Catal. Lett.* **112** 129–32
[58] Traylor M J, Pavlovich M J, Karim S, Hait P, Sakiyama Y, Clark D S and Graves D B 2011 Long-term antibacterial efficacy of air plasma-activated water *J. Phys. D: Appl. Phys.* **44** 472001
[59] Chen J G *et al* 2018 Beyond fossil fuel–driven nitrogen transformations *Science* **360** eaar6611
[60] Li S, Medrano J A, Hessel V and Gallucci F 2018 Recent progress of plasma-assisted nitrogen fixation research: a review *Processes* **6** 248
[61] Li Z, Nie L, Liu D and Lu X 2022 An atmospheric pressure glow discharge in air stabilized by a magnetic field and its application on nitrogen fixation *Plasma Process. Polym.* **19** e2200071
[62] Liu J, Nie L, Liu D and Lu X 2023 Plasma for nitrogen fixation by using N_2/O_2 mixture: reaction pathway, energy flow, and plasma reactor *Plasma Process. Polym.* **21** e2300153
[63] Muzammil I, Lee D H, Dinh D K, Kang H, Roh S A, Kim Y-N, Choi S, Jung C and Song Y-H 2021 A novel energy efficient path for nitrogen fixation using a non-thermal arc *RSC Adv.* **11** 12729–38
[64] Vervloessem E, Aghaei M, Jardali F, Hafezkhiabani N and Bogaerts A 2020 Plasma-based N_2 fixation into NO_x: insights from modeling toward optimum yields and energy costs in a gliding arc plasmatron *ACS Sustain. Chem. Eng.* **8** 9711–20